J. Fluid Mech. (1987), *vol.* 175, *pp.* 119–142
Printed in Great Britain

On the generation of high-amplitude wall-pressure peaks in turbulent boundary layers and spots

By ARNE V. JOHANSSON†, JEN-YUAN HER AND JOSEPH H. HARITONIDIS

Department of Aeronautics and Astronautics, Massachussetts Institute of Technology, Cambridge, MA 02139, USA

(Received 11 February 1986)

The coupling between high-amplitude wall-pressure peaks and flow structures, especially in the near-wall region, was studied for a zero-pressure-gradient turbulent-boundary-layer flow and for the flow in the interior of artificially generated turbulent spots. By use of an 'enhanced' conditional averaging technique it was shown that buffer region shear-layer structures are to a high degree responsible for the generation of large positive wall-pressure peaks. The relation was proved to be bi-directional in that strong shear layers were shown to accompany positive pressure peaks and correspondingly that large pressure peaks were associated with shear-layer structures detected in the buffer region. This also indicates a link between the wall-pressure peaks and turbulence-producing mechanisms. The pressure-peak amplitude was found to scale linearly with the velocity amplitude of the generating flow structure, indicating that a dominating role here is played by the so-called turbulence–mean shear interaction. The large negative wall-pressure peaks were found to be associated primarily with sweep-type motions. All essential features of the relation between wall-pressure peaks and flow structures in artificially generated spots in a laminar boundary layer were found to be identical to those in the equilibrium turbulent boundary layer.

1. Introduction

The generation of wall-pressure fluctuations beneath a turbulent boundary layer is coupled to the dynamics of the velocity fluctuations throughout the entire boundary layer, both through interaction between the latter and the mean shear and through nonlinear interaction of the velocity fluctuations with themselves. The roles of these different types of processes for the generation of wall-pressure and the question of location of the major pressure sources have been investigated both theoretically and experimentally in a number of studies. For a review of earlier work in this field see Willmarth (1975).

The high values of propagation velocities (typically 80% of the free-stream velocity) for the low wavenumber part of the wall pressure is one indication that a significant contribution to the long-time r.m.s.-value originates from flow structures in the outer region of the boundary layer. However, of particular interest, from the point of view of e.g. sound generation, is the occurrence of high-amplitude peaks, i.e. peaks several times larger than the long-time r.m.s.-value (p_{rms}). Many of the efforts in recent studies have focused on the propagation characteristics (Schewe 1983) of

† Permanent address: Department of Mechanics, The Royal Institute of Technology, S-100 44 Stockholm, Sweden.

large peaks, and their relation to organized motions in the near-wall region of pipe (Dinkelacker & Langenheineken 1983) and boundary-layer flows (Thomas & Bull 1983). Although many of the detailed questions have remained unanswered, some qualitative correspondence between near-wall region flow structures and large positive pressure peaks has been established from these studies.

The present work is aimed at clarifying and substantiating the information on flow structures predominantly responsible for the high amplitude wall-pressure peaks beneath a zero-pressure-gradient turbulent boundary layer, the location of these structures and their relation to the turbulence production mechanisms. For this purpose, results from conditional sampling of events characterized by the occurrence of high-amplitude pressure peaks were compared with those obtained by detection of shear layers at different positions in the boundary layer. The latter was achieved by use of the Variable-Interval Time-Averaging (VITA) technique (Blackwelder & Kaplan 1976). In order to enable a comparison of a more quantitative nature to be made, an enhancement technique was used to remove most of the phase jitter associated with the conditional averaging process.

There is a gross similarity between the flow in a turbulent boundary layer and that in the interior of an artificially generated turbulent spot in a laminar boundary layer (see e.g. Wygnanski, Sokolov & Friedman 1976). A vast amount of data exist on the structure of the flow in the spot, and its propagation and spreading characteristics (see e.g. the review paper by Riley & Gad-el-Hak 1985). Cantwell, Coles & Dimotakis (1978) inferred the wall-pressure signature along the symmetry line of the spot from velocity data. Aside from differences in amplitudes, this inferred signature is in qualitative agreement with experimental results of Coles & Savas (1979). However, the spot-pressure signature measured by Mautner & Van Atta (1982) is significantly different. The question of the wall-pressure signature of the spot was addressed also in the present work. The relation between flow structures and wall-pressure peaks in the interior of the spot was investigated and compared with the results for the turbulent-boundary-layer case. To the present authors' knowledge no results have previously been reported on the generation of high-amplitude wall-pressure peaks in the interior of spots.

2. Experimental procedure and flow conditions

The experiments were carried out in the Low Turbulence Wind Tunnel of the Department of Aeronautics and Astronautics (MIT). The test section is 5 m long, 0.6 m wide and 1.2 m high. A zero-pressure-gradient turbulent or laminar boundary layer is developed along a vertically placed flat aluminium plate, which is located near one of the vertical walls of the test section. The maximum free-stream velocity (U_∞) is about 40 m/s, but for the present experiments a value of 10 m/s was chosen, for both the turbulent-boundary-layer case and the spot case, as a compromise among opposing requirements for low tunnel noise, high free-stream dynamic pressure and large turbulence scales. At this velocity the free-stream turbulence level was below 0.05%. Other basic parameters of the flow and details of the wind tunnel are given in Mangus (1984).

Velocity measurements were carried out with small hot-wire probes. Both single sensors and cross-wire probes were used and the length to diameter ratio was, in all cases, above 200. They were operated at an overheat ratio of 1.6, giving a frequency response of at least 20 kHz. The hot-wire drift was checked after each run, and was typically less than 0.5%.

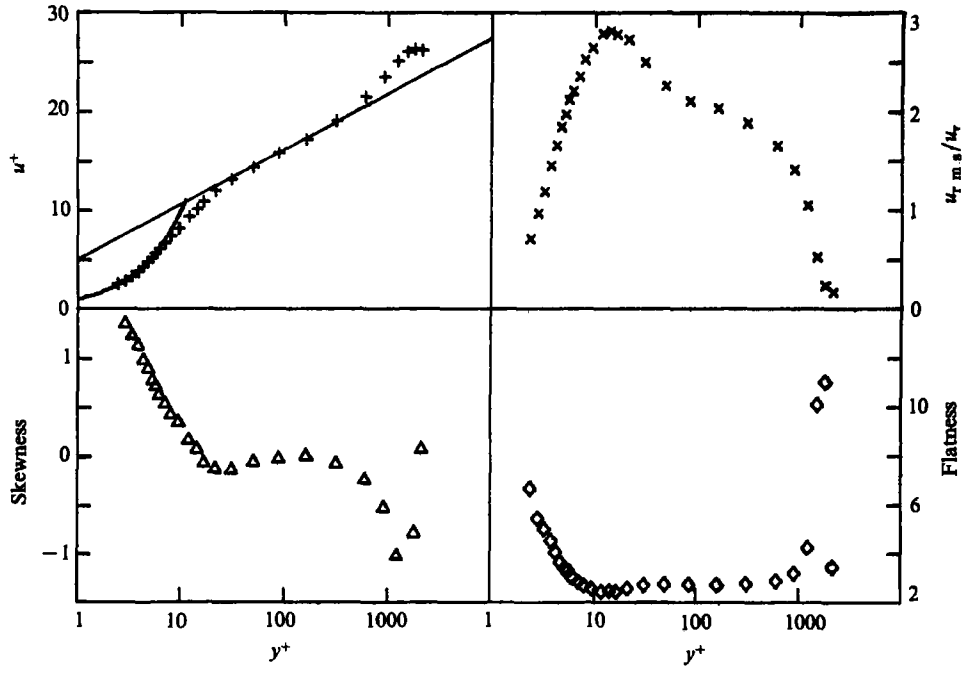

FIGURE 1. Profiles of mean velocity, streamwise turbulence intensity, skewness and flatness in a turbulent boundary layer. $U_\infty = 10.2$ m/s, $x = 4.0$ m. Straight line in mean velocity plot represents $u^+ = (1/0.41)\ln y^+ + 5.0$.

The hot wire was positioned using a three-degree of freedom computer-controlled traverse and data were acquired through a 16-channel, 12-bit A/D converter with simultaneous sample and holds. The data acquisition and the hot-wire traverse were controlled by a PDP 11/55 computer.

A flush-mounted Bruel and Kjaer condenser microphone, with a diameter of 2.5 mm, was used for all the wall-pressure measurements. It has a flat frequency response from 18 Hz to 15 kHz. The pressure signals were amplified by a Bruel and Kjaer 2619 microphone follower and an Ithaco 432 preamplifier before A/D conversion. The ratio of mean-square values of the pressure beneath the turbulent boundary layer and that of the noise without flow was found to be about 10.

2.1. *The turbulent boundary layer*

The turbulent-boundary-layer measurements were carried out at a streamwise position (x) of 4 m downstream of the leading edge, where the momentum thickness (Θ) was 7.29 mm at $U_\infty = 10.2$ m/s, giving a Reynolds number (Re_Θ) of 4940. In this case the boundary layer was tripped by means of a 5 cm wide strip of (no. 36 open coat) sandpaper placed 5 cm downstream from the leading edge. The friction velocity, u_τ, was determined from a Clauser plot that gave a U_∞/u_τ ratio of 26.3. The inner lengthscale (l_*), defined as ν/u_τ, where ν is the kinematic viscosity, was 0.039 mm, whereas the inner timescale ($t_* = \nu/u_\tau^2$) was 0.101 ms. The length of the single sensor hot wire 0.25 mm, which corresponds to about $7l_*$. Non-dimensionalization with inner variables will, in what follows, be denoted by a + superscript.

Distributions of the first four statistical moments of the streamwise velocity (u) are shown in figure 1. Effects of heat conduction to the wall were minimized by

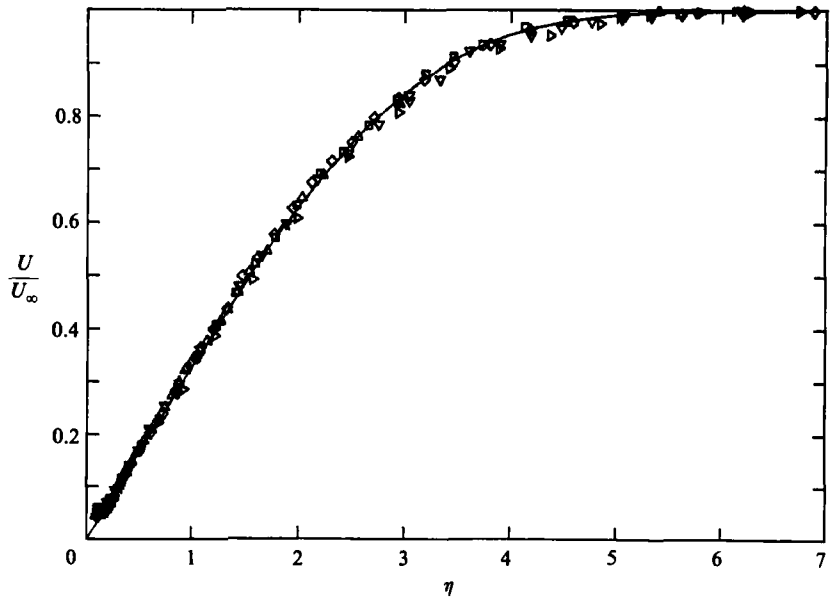

FIGURE 2. Laminar boundary-layer profiles for $U_\infty = 10$ m/s and various positions along the plate, plotted in similarity coordinates ($\eta = y(U_\infty/\nu x)^{\frac{1}{2}}$). Virtual origin of boundary layer at $x = -0.03$ m. ——, Blasius profile; □, $x = 0.28$ m; ◇, $x = 0.55$ m; △, $x = 0.80$ m; ▽, $x = 1.05$ m; ▷, $x = 1.54$ m.

measuring over a Plexiglas insert, thereby enabling accurate measurements even in the viscous sublayer. The quantities in figure 1 conform well to standard boundary-layer values. For instance, the maximum turbulence intensity is $2.83u_\tau$, which agrees well with the results of e.g. Purtell, Klebanoff & Buckley (1981), and the data of Johansson & Alfredsson (1983) (see their figure 7).

For all cases reported here, the hot wire was placed immediately downstream of the pressure transducer, i.e. about 2 mm ($50l_*$) from the centre of the microphone, and at various positions in the boundary layer from the viscous sublayer to the outer region. The microphone diameter here corresponds to approximately $65l_*$. The digitizing rate for both the velocity and the pressure was 10 kHz, giving an interval between samples of about $1.0t_*$. The total sampling time for each set of data was 13.4 s, or about 1900 δ/U_∞, where δ is the boundary-layer thickness.

2.2. *The turbulent spot*

A major portion of the pressure measurements for the spot case were carried out at 1.54 m from the leading edge of the plate. The laminar-boundary-layer profiles were measured at various streamwise positions along the plate and were found to conform well to the Blasius solution (figure 2). The spots were triggered at a position 29 cm from the leading edge by blowing a small (1 mm diameter) air jet into the boundary layer, by means of a pulse from a loudspeaker connected to a hole in the plate. The amplitude and duration of the pulse could be controlled. It was triggered from the computer and data sampling started after a chosen time delay. Good repeatability of the spots was obtained in this manner and no other condition was needed for construction of ensemble averages of the spot velocity and pressure signatures. Ensemble averages were constructed from sets of 500 spots and the time between spot triggerings was chosen to be 1 s, which was sufficient to ensure relaxation of the flow back to laminar conditions between successive spots.

The time between samples was chosen as 0.21 ms, which corresponds to about $2.6t_*$ with the U_∞/u_τ ratio estimated from the flow in the interior of the spot (see § 4). The non-dimensional diameter of the microphone was not substantially different from that in the boundary-layer case.

3. Results: the turbulent boundary layer

The major portion of the results presented in the following concerns the generation of high-amplitude wall-pressure peaks and their relation to flow structures in the near-wall region. Some basic features of the pressure measurements and their limitations will first be discussed, particularly concerning the spatial resolution achieved with the transducer used.

The effects of finite transducer size on wall-pressure fluctuation measurements have attracted attention from a number of investigators (see e.g. Corcos 1963; Willmarth & Roos 1965 and Bull & Langeheineken 1981) and were recently studied experimentally in detail by Schewe (1983) for a relatively low Reynolds number. In the present case (with $d^+ = 65$) the intensity of the pressure fluctuations normalized by the free-stream dynamic pressure (q) attained a value of 0.0078 ($p_{\rm rms}/\tau_{\rm w} = 2.70$), whereas the skewness and flatness factors were found to be 0.05 and 3.8, respectively. This is in good agreement with Schewe's results for similar non-dimensional transducer size. One may also mention here that Bull & Langeheineken (1981) proposed that there is a genuine Reynolds-number dependence of the quantity $p_{\rm rms}/q$. Their results indicate that the intensity should be approximately 0.007 at the present Reynolds number and transducer size, as compared to 0.008 at the Reynolds number used by Schewe.

The r.m.s.-value for $d^+ = 80$ was shown by Schewe to be about 20% lower than that for a vanishingly small transducer. Hence, all the small scales are not resolved in the present case, but of more primary interest here is to what extent the dominant high-amplitude peaks are resolved. In Schewe's case, peaks with an amplitude larger than three times the long-time r.m.s.-value were found to have an average streamwise lengthscale of $145l_*$, indicating that the resolution in the present case is reasonable for the purpose in question. However, the spanwise spatial resolution is somewhat worse and may cause some attenuation of pressure amplitudes.

Events corresponding to high-amplitude pressure peaks were detected for both positive and negative peaks for various threshold levels, k, i.e. an event is considered to occur when the amplitude of the pressure exceeds $kp_{\rm rms}$. The reference time, t_i, for each event was taken as its mid-point. Conditional averages of the pressure could then be constructed as

$$\langle p(\tau)\rangle = \frac{1}{N}\sum_{i=1}^{N} p(t_i+\tau), \tag{1}$$

where τ is a time relative to the reference or detection time. Velocity patterns were computed similarly using the same reference times. Non-dimensional averages will be denoted by star superscript, and are in all cases normalized by the respective r.m.s. value. The pressure signatures for this conditional averaging scheme will also be divided by the threshold k.

Figure 3 shows wall-pressure patterns for positive and negative peaks detected with various threshold levels. The patterns collapse with the normalization used, which was also found to be true for the corresponding velocity patterns when normalized with k. The duration of the peaks, as seen by a fixed probe, can be estimated to 10–$15t_*$, to be compared with the value $12t_*$ given by Schewe (1983). The peak amplitude of

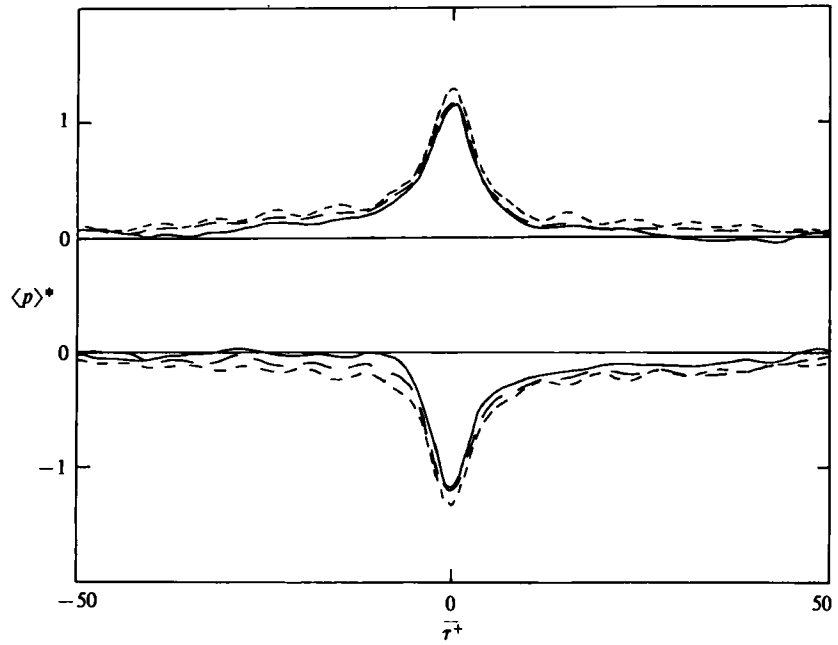

FIGURE 3. Conditional averages of p_w for positive and negative pressure-peak events (——, $k = 1.5$; – –; $k = 2.5$; - - -, $k = 3.5$) in a turbulent boundary layer ($x = 4$ m, $U_\infty = 10.2$ m/s).

the non-dimensional pressure patterns is about 1.2 for all three threshold levels, signifying the fact that the number of events detected decreases rapidly with increasing threshold level. All events with amplitudes corresponding to higher k-values than the threshold used are included in the ensemble average. However, since the number of events decreases so rapidly with increasing k, only a small interval of amplitudes will contribute significantly to the ensemble average, thus causing the patterns in figure 3 to collapse. The frequency of occurrence of pressure peaks was found to decrease exponentially with increasing threshold level (figure 4). (It should be noted that this is the same type of behaviour as for the frequency of occurrence of uv peaks (see Alfredsson & Johansson 1984), and of VITA events (Johansson & Alfredsson 1982)). A comparison of the pressure results with those of Schewe (for $k = 3.2$) yields reasonable agreement. The frequency of occurrence (scaled with inner variables) of positive peaks is in his case approximately 0.0011 (0.0015 for negative), which is just slightly higher than the present results. This may probably be ascribed to spatial resolution effects, assuming inner scaling for their frequency of occurrence.

From the width of the pressure patterns in figure 3, and the frequency of occurrence in figure 4, one may estimate that peaks with an amplitude larger than $2.5p_{rms}$ occur during roughly 6% of the total time. Their contribution to the long-time r.m.s. value amounts to about 18%. The threshold value of 2.5 will be used in the following, unless otherwise stated, in the detection of high-amplitude pressure peaks.

Aside from the pressure-peak detection scheme, the so called VITA-technique (Blackwelder & Kaplan 1976) was also used to study the origin of dominant wall-pressure peaks, and their relation to 'deterministic' events in the flow. The VITA detection (discussed in more detail by, e.g. Johansson & Alfredsson 1982) was applied to the streamwise velocity signal at various y-positions, whereafter conditional averages of the velocity component(s) and the pressure were constructed as in (1).

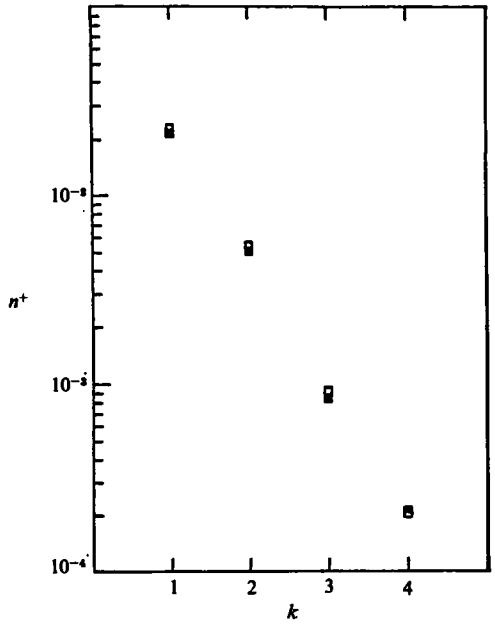

FIGURE 4. Frequency of occurrence (in wall units) of pressure-peak events (□, positive peaks; ■, negative peaks) *vs.* threshold level. $x = 4$ m.

The reference time (t_i) for each event is also here taken as its mid-point. A VITA event is considered to occur when

$$\text{var} = \frac{1}{T}\int_{t-\frac{1}{2}t}^{t+\frac{1}{2}T} u^2(s)\,\mathrm{d}s - \left(\frac{1}{T}\int_{t-\frac{1}{2}T}^{t+\frac{1}{2}T} u(s)\,\mathrm{d}s\right)^2 > K u_{\text{rms}}^2, \tag{2}$$

where var is the short-time variance over an averaging time T, and K is the threshold level. Accelerating and decelerating types of events can be distinguished and were treated seperately. For most cases presented in the following figures a threshold of 1.0 was used, and the averaging time was chosen to be $24t_*$, which is the value for which the maximum number of accelerating events are detected (in the buffer region). The conditional averages were made non-dimensional with the respective r.m.s. value.

The VITA technique detects sharp shear layers, the timescale of which, as seen by a fixed probe, is essentially the averaging time used in the detection. The T value therefore also influences the timescale of the conditionally obtained pressure average. The strong shear layers in the near-wall region are caused by lift-up (ejection) of low-speed fluid from positions closer to the wall and are dynamically important in the turbulence-production process.

With the above choice of parameters in the VITA technique we obtained about the same frequency of occurrence of events detected at $y^+ = 15$, as that of positive pressure-peak events detected with $k = 2.5$, which facilitates comparisons between results for the two techniques.

3.1. *Positive pressure peaks and buffer region shear layers*

Figure 5 illustrates the relation between high-amplitude positive pressure peaks and structures in the flow by means of conditional averages of the wall pressure and the streamwise velocity at various distances from the wall. The wall-pressure and velocity

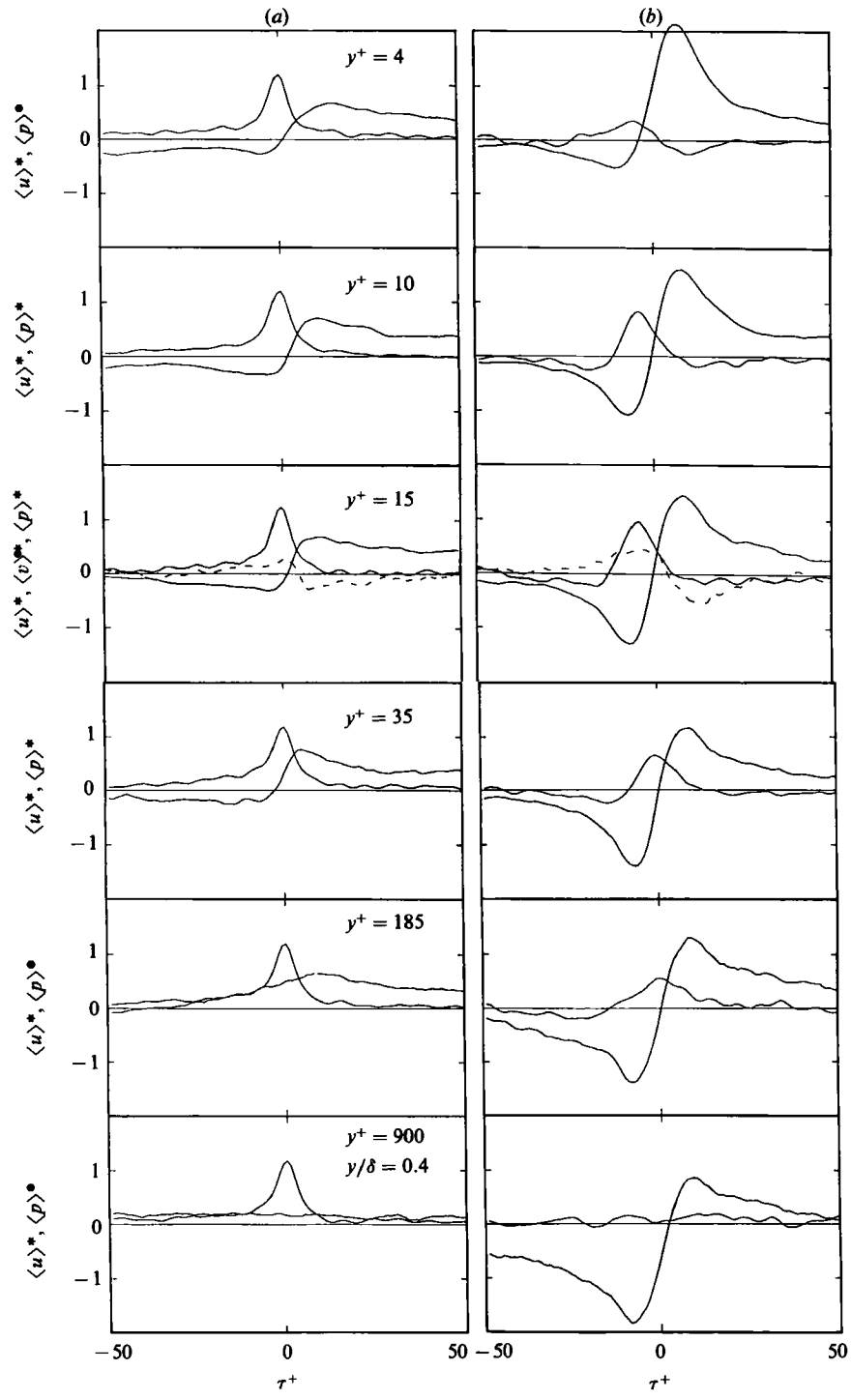

FIGURE 5. Conditional averages of p_w and u at various y^+ positions, and v (- - -) at $y^+ = 15$, for (*a*) detection of positive pressure peaks ($k = 2.5$), and (*b*) VITA detection of accelerating events ($k = 1.0$, $T^+ = 24$). $\langle u\rangle^* = \langle u\rangle/u_{rms}$, and $\langle p\rangle^* = \langle p\rangle/kp_{rms}$ in (*a*) and $\langle p\rangle/p_{rms}$ in (*b*). τ^+ denotes time, in wall units, relative to the detection time. $x = 4$ m.

patterns in figure 5(*a*) were obtained with the reference times set by the pressure-peak detection, which means that the pressure patterns are essentially the same, the only difference being that they were obtained from different sets of data. (This is of course not so in figure 5*b*.) The velocity patterns in figure 5(*a*) indicate that the positive wall-pressure peaks are related to sharp shear layers in the buffer region. This is most clearly seen around $y^+ = 15$, with a sharp velocity increase occurring slightly after the detection time. For this correspondence to have any substantial significance it should be 'bi-directional', i.e. one should also be able to obtain pressure patterns similar to those in figure 5(*a*) by detecting the shear layers from the streamwise velocity signal. This was investigated through detection of shear layers at various y^+-positions by means of the VITA technique (figure 5(*b*)). A definite positive pressure peak is seen in figure 5(*b*) to be associated with these events in the buffer region, where there is also a general qualitative similarity between the conditional averages obtained with the two techniques. Further out in the log-region ($y^+ = 185$) and in the outer region ($y/\delta = 0.4$) this is no longer true and there is indeed very little wall-pressure activity associated with shear layers detected in the outer region.

The general resemblance between the conditional averages obtained with VITA detection at $y^+ = 15$ and those obtained by detection of positive pressure events is seen in figure 5 to extend also to the v-component (measured with an X-probe). The choice of VITA-detection parameters ($K = 1.0$ and $T = 24t_*$) results in an amplitude of the pressure pattern associated with VITA events of about $1.0p_{\mathrm{rms}}$, to be compared with an amplitude of about $3p_{\mathrm{rms}}$ (1.2 times a threshold of 2.5) found with the direct pressure-peak detection. Since the frequency of occurrence of events is roughly the same, this would imply a rather poor correspondence between the information obtained in these two ways, but this is, to a considerable extent, due to phase-jitter in the conditional averaging process. This problem will be discussed in some detail later, as well as methods to alleviate it.

One should remember when interpreting the results in figure 5 that the phase relationship between velocity and wall-pressure patterns should be corrected for the streamwise separation between the microphone and the hot wire. With a propagation velocity of 11 u_τ for the pressure pattern (see e.g. Schewe 1983), it should be shifted approximately $5t_*$ to the right. The pressure maximum would thereby coincide with the centre of the shear layer.

A noticeable difference between the pressure patterns in figure 5(*a*) and (*b*) ($y^+ = 15$), is the lack of negative pressure regions around the peak for the pattern obtained with direct pressure-peak detection. This was found to be mainly caused by a relatively small number of detections associated with very low frequency pressure fluctuations. Removal of these, by high-pass filtering of the pressure signal with a lower cut-off frequency of 0.01 in inner units, resulted in a pattern very similar to that associated with the VITA events. Filtering was not applied for the results presented in the following, but this effect should be kept in mind when comparing results of the two techniques.

To further investigate the relation between positive pressure-peaks and shear-layers in the buffer region, the maximum amplitude, within a region of $\pm 25t_*$ around the VITA-detection time, was determined for each event in the ensemble average (of figure 5(*b*), $y^+ = 15$). For this case, a pressure-detection level of $2.33p_{\mathrm{rms}}$ would give exactly the same number of events as the VITA technique (with $K = 1.0$ and $T = 24t_*$). Approximately 35 % of these pressure peaks were found to occur within the above specified window and more than half of the VITA detections were found to be associated with a peak larger than $2p_{\mathrm{rms}}$. Also, the large pressure peaks were found to occur predominantly alone, or accompanied only by peaks of a more

moderate amplitude. Only for 7% of the events was there a double peak with an amplitude larger than $2.33p_{\rm rms}$ within the $\pm 25t_*$ window.

Some perspective on the generality of the results in figure 5 is given by comparison with the work of Langeheineken (1981) (see also Dinkelacker & Langeheineken 1983) in a low-Reynolds-number ($Re_\theta = 346$) pipe flow. He used a pressure transducer of the same kind as in the present study, but with a pinhole mounting, and applied pressure-peak detection as in the present case. He recognized a clear relation between high positive pressure peaks and rapid increases in the streamwise velocity, as seen by a fixed probe. The velocity patterns obtained in that flow resemble fairly closely those obtained in the present boundary-layer study (figure 5(*a*)). He was also able to substantiate the coupling between positive pressure peaks and shear layers by examining events associated with large values of the temporal derivative of u.

In this context it is also interesting to make a comparison with the work of Thomas & Bull (1983) who searched for 'characteristic' wall-pressure patterns associated with the bursting process in a turbulent boundary layer. They used a transducer with a diameter that, in inner units, was close to the one in the present study. They investigated the possibility of relationships between the low- and high-frequency parts of the pressure signal and detected peaks in the smoothed rectified high-frequency part. The resulting conditional average is characterized by a rapid decrease of the pressure at the detection time. The amplitude of this pattern is, however, fairly low (less than $0.4p_{\rm rms}$). Its streamwise extent was estimated to 1.5–2.0 times the boundary-layer displacement thickness, or about $470l_*$, and the propagation velocity was found to be $0.67U_\infty$ or about $19u_\tau$. All in all, these characteristics are quite different from those found for large pressure peaks in the studies of Schewe (1983) and Langeheineken (1981), as well as the present study. Thomas & Bull concluded, from the value of the propagation velocity, for example, that the observed pressure patterns are related to flow structures located in the logarithmic region, around $y^+ = 250$. They also used a conditional sampling technique based on the detection of peaks in the smoothed rectified high-pass filtered velocity at $y^+ = 30$. From this they obtained velocity patterns of similar character to VITA signatures and a pressure pattern again characterized by a rapid decrease, but of very small amplitude (about $0.2p_{\rm rms}$). However, from considerations of the relationship between the pressure and the streamwise derivative of v (the turbulence–mean shear interaction) they concluded that representative pressure patterns associated with shear layers should be dominated by a positive peak that is fairly symmetric around its maximum. This is in accordance with the present results.

Kim (1983) applied the VITA-detection technique to numerical simulation data of turbulent channel flow, and found that these events, when detected in the buffer region, are associated with a pressure signature characterized by a positive peak surrounded by small-amplitude negative regions. These are in qualitative agreement with the present results, but their spatial scale (or duration) is much larger than in the present case. This can be ascribed to spatial resolution problems in the numerical simulation. A much finer resolution (and somewhat different numerical technique) was used by Kim & Moin (1986) in a numerical simulation without subgrid-scale modelling. However, no pressure results have yet been presented from that computation.

3.2. *Enhanced conditional averaging by removal of 'phase-jitter'*

To be able, in some quantitative sense, to determine the origin of high-amplitude wall-pressure peaks, one needs a conditional sampling scheme that, from detection

on some characteristics of a flow structure, is able to educe an associated wall-pressure pattern of such an amplitude that it is at least comparable with that obtained by direct pressure-peak detection. This is only to a very moderate degree true for the previously mentioned boundary-layer and pipe-flow studies, as well as for the results in figure 5. To a considerable extent this is due to phase-jitter in the conditional averaging process. For instance, the true maximum amplitude of the pressure patterns associated with VITA events in the buffer region is substantially higher than that depicted in figure 5 (*b*). This is due to the variation in the time difference between the occurrence of the pressure-peak mid-point and the VITA-detection time. This type of problem has been addressed by, e.g. Zilbermann, Wygnanski & Kaplan (1977), Blackwelder (1977) and Hussain (1983). In Zilbermann *et al.* (1977), a cross-correlation technique was successfully used to remove effects of phase-jitter in an attempt to extract information about a turbulent spot merging into a fully turbulent region. A similar technique was also used by Lindberg *et al.* (1984) in a study of the flow field outside a turbulent spot. The cross-correlation approach was adopted also in the present study to 'align' pressure (and $v-$) patterns associated with VITA events, and velocity patterns associated with pressure-peak detections.

In the iterative alignment procedure for the former case the conditional averages are first constructed in the usual manner, whereafter the cross-correlation of each $p-$ (or $v-$) realization and the conditional average is computed over a time window around the detection time, or around a time displaced a chosen amount from the detection time. This window was here chosen to be $50t_*$ long. Each realization is given an appropriate time shift determined by the displacement of the maximum in the cross-correlation. This time shift is then used for alignment when the realizations are added to form a new conditional average. The procedure can then be repeated, although most of the phase-jitter is removed already in the first iteration. The procedure is exactly the same to align velocity patterns in the pressure-peak detection case. For an ideal situation where the realizations are identical, but displaced randomly around the detection time, the final aligned average will give a completely true picture of the event, but also when the individual realizations are moderately different, as in the cases that will be treated here, the method works quite well to give a representative picture of the event.

The resulting conditional averages after two iterations of alignment in figure 6 (*a*) and (*b*) should be compared with the corresponding patterns in figure 5 ($y^+ = 15$). Most of the phase-jitter is removed in the first step, especially for the alignment of velocity patterns for which the results after one and two iterations were identical. The total time shift was for most of the events quite small. Roughly 75 % of the events in figure 6 (*a*) and (*b*) were given time shifts smaller than $10t_*$.

The results for positive pressure-peak events in figure 6 (*a*) show a substantially increased amplitude of the u-pattern after alignment. Indeed, this amplitude is quite comparable to that obtained by the VITA detection. Also, figure 6 (*b*) shows that the true amplitude of the pressure patterns associated with VITA-detected shear layers in the buffer region is almost a factor of two larger than that obtained without alignment. Thus, the correspondence is much closer than is revealed without alignment. One should, in this comparison, remember that the detection scheme parameters were chosen to give approximately the same frequency of occurrence of events for both techniques. Also, the pressure signature should be shifted approximately $5t_*$ to the right to correct for the streamwise separation between the two types of sensors.

The smearing effect of phase-jitter makes the slope of the streamwise velocity

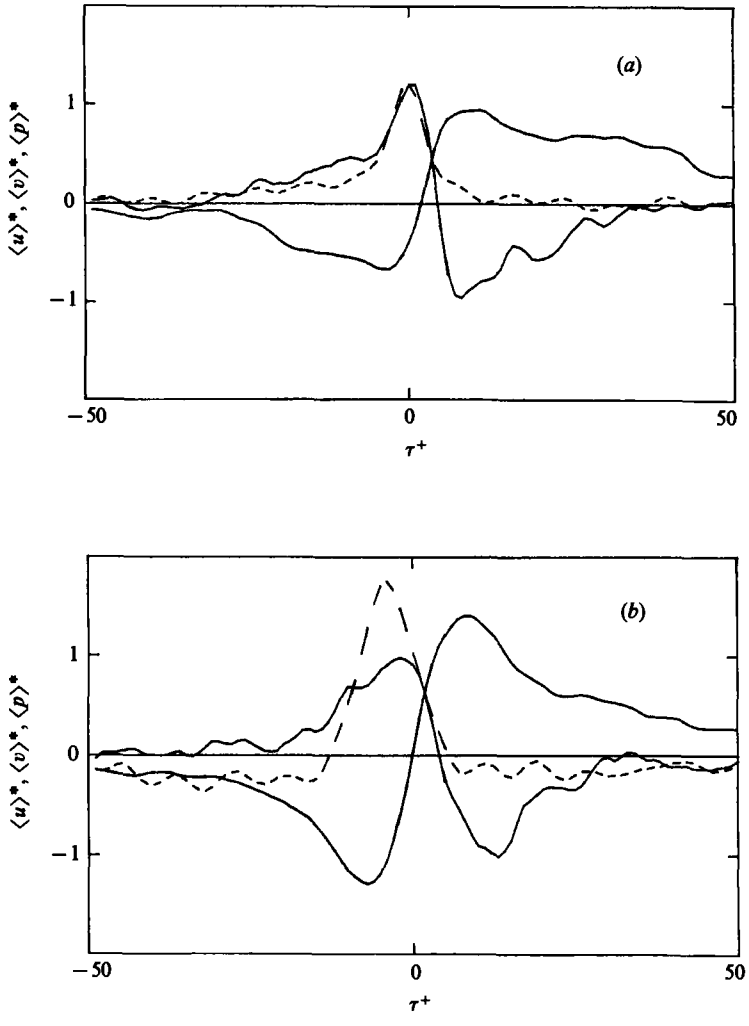

FIGURE 6. Aligned (two iterations) conditional averages of p_w (dashed line) and, u and v at $y^+ = 15$. (a) detection of positive pressure peaks ($k = 2.5$), (b) VITA detection of accelerating events ($K = 1$, $T^+ = 24$). $x = 4$ m.

pattern (figure 6(a)), at the detection time, smaller than the true value and one would hence estimate too large a timescale from this slope without alignment. Correspondingly, one would over-estimate the thickness of the shear layer. It is interesting to note that after alignment the shear-layer timescale, as estimated from the slope, is close to that seen from the VITA average in figure 6(b). One must here remember that the 'slope-timescale' of the VITA average is essentially proportional to the averaging time used in the VITA detection, as shown by Johansson & Alfredsson (1982). However, in this case the averaging time used was that which gave the largest number of detections. Hence, the duration of the most probable VITA events is roughly the same as the 'slope-timescale' in figure 6(a), which can be seen as a characteristic timescale for the pressure-peak-generating shear layers in the buffer region. Indeed, figure 6(a, b) clearly indicates that these shear layers can be regarded as dominant contributors to the large-amplitude peaks.

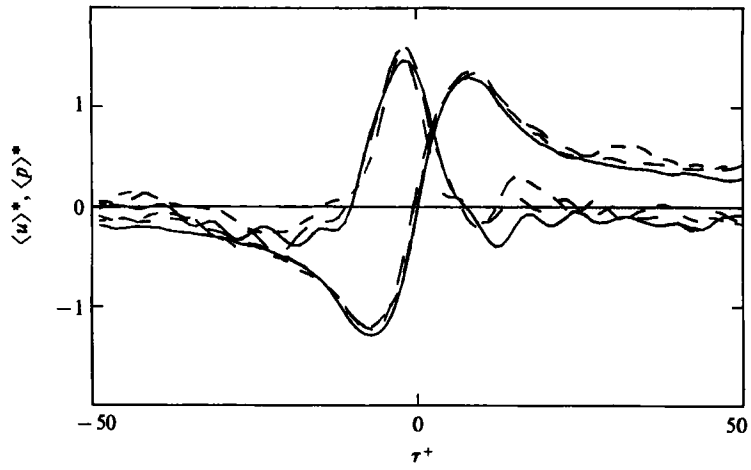

FIGURE 7. Aligned (two iterations) conditional averages of p_w, and u at $y^+ = 15$ for VITA detection with various threshold levels, ——, $K = 1.0$; – –, $K = 1.5$; - - -, $K = 2.0$. $T^+ = 24$. Note that the u- and p-averages here have been normalized with $K^{\frac{1}{2}}$ times the respective r.m.s. value.

The amplitude of the u-pattern has been shown to be proportional to the square root of the threshold used in the VITA detection (see e.g. Johansson & Alfredsson 1982). This was here also found to be true for the associated pressure patterns, especially after alignment (figure 7). Figure 7 also reveals that the relatively rare events detected with $K = 2$ generate a wall-pressure peak of as high an amplitude as $2.3p_{\text{rms}}$. The collapse for normalization with the square root of K implies that the amplitude of the pressure peak is linearly related to the amplitude of the velocity pattern, which in turn indicates that the generation of high-amplitude pressure peaks is predominantly governed by turbulence–mean shear interaction. This can be seen from the formal solution for the fluctuating component of the wall-pressure field, which can be written as a Poisson integral (over the upper half-space, $x_2 = y > 0$) with a source term, q,

$$q = 2\frac{\partial U_i}{\partial x_j}\frac{\partial u_j}{\partial x_i} + \frac{\partial^2(u_i u_j - \overline{u_i u_j})}{\partial x_i \partial x_j}.$$

The two terms in the above expression represent (in tensor notation) the so called turbulence–mean shear interaction and the turbulence–turbulence interaction, respectively. The former depends linearly on the velocity fluctuations, and for a parallel two-dimensional flow it becomes proportional to $\partial v/\partial x$. Hence, for a signal from a fixed probe one should expect a positive pressure peak to be associated with a large negative value of $\partial v/\partial t$, which for the shear-layer signatures presented in the previous figures is associated with a sharp increase in u. Also, one should expect this correspondence to be accentuated in the region where the mean velocity gradient is large. This can be further illustrated by applying the VITA detection to the v-signal at $y^+ = 15$ with a 'negative slope criterion' (VITA on v has previously been tried by Alfredsson & Johansson 1984). The results for p were found to be sensitive to phase-jitter in this case, resulting in a small p-amplitude without alignment. After alignment (figure 8), on the other hand, the results were comparable with those for VITA on u detection. The chosen threshold in figure 8 was higher than that used for u in figures 5 and 6 since a larger number of events are detected in v for the same K-value. Also included in figure 8 is the pressure pattern shifted in time to correct

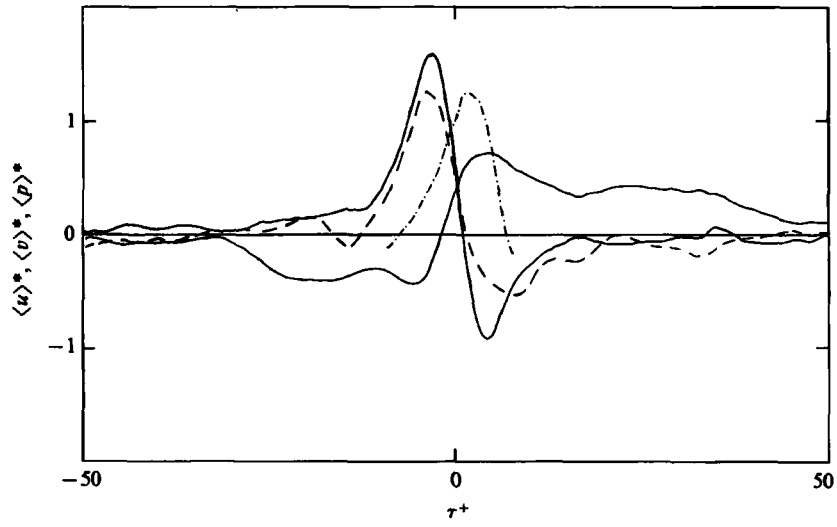

FIGURE 8. Aligned (two iterations) conditional averages of p_w (dashed curve), and u and v at $y^+ = 15$ for VITA detection of decelerating events in the v signal ($K = 2$, $T^+ = 12$). –·–·–, pressure pattern shifted in time to correct for the streamwise separation between the hot wire and the pressure transducer.

for the distance between the pressure transducer and the hot wire. The maximum pressure amplitude is then seen to coincide with the centre of the shear layer.

3.3. *Negative wall-pressure peaks and sweep motions*

Large negative pressure peaks occur approximately as frequently as the positive ones for the same amplitude (see figure 4). Also, their duration or streamwise extent, is about the same as that for the positive peaks (figure 3). However, for the negative peaks there is no apparent coupling to shear layers in the buffer region. Instead, the associated velocity patterns are characterized by a period of high streamwise velocity (figure 9) around the detection time. This becomes even clearer after application of the alignment procedure (figure 9, $y^+ = 15$). The associated period of high streamwise velocity would indicate that they are coupled to sweep-type motions. This was substantiated by two-component velocity measurements (figure 10). As explained in §3.1, the p-pattern should be shifted approximately $5t_*$ to depict the correct phase relationship between velocity and pressure signatures. Hence, the maximum negative pressure occurs during a period of decreasing u and increasing v, suggesting that negative pressure peaks should also exhibit a coupling to decelerating VITA events (detected in u). This coupling was, however, found not to be as clear as that between positive peaks and accelerating VITA events.

Sometimes large negative and large positive pressure peaks occurred together. The case where the negative peak succeeded the positive appeared to be somewhat more probable than the reverse, although both were fairly rare. Events associated with the former case, which corresponds to a local adverse pressure gradient, could be detected by applying the VITA technique with a 'negative slope criterion' to the pressure signal. Like the single positive pressure peaks, these events were found to be correlated (although not as clearly) to shear-layer-like flow structures in the buffer region.

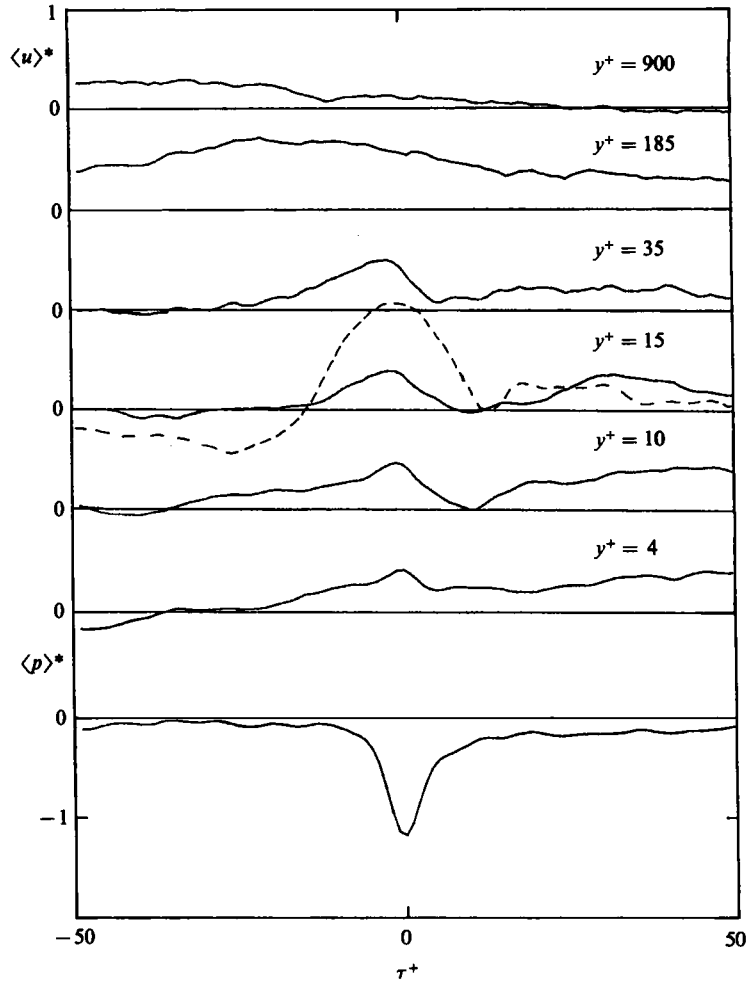

FIGURE 9. Conditional averages of p_w, and u at various distances from the wall for detection of negative pressure peaks ($k = 2.5$). Aligned u pattern (- - -) at $y^+ = 15$ is also included.

4. Results: the turbulent spot

The flow in the interior of a turbulent spot is in many respects similar to the flow in an equilibrium turbulent boundary layer. It has, for example, been shown (Wygnanski *et al.* 1976) that the mean velocity profile in the spot exhibits the same type of logarithmic behaviour as in the turbulent boundary layer. However, in the former case there is a slow variation in the streamwise direction of time–mean characteristics such as mean velocity at different y-levels, skin friction and wall-pressure. Streamwise variations in, for example, the mean velocity will of course be much smaller than in the direction normal to the wall, since the spot is very flat. The results presented in the following were taken for spots at an x-position of 1.54 m from the leading edge of the plate ($x_{trig} = 0.29$ m), and for the same free-stream velocity as in the boundary-layer case. The streamwise dimension of the spot is here roughly a factor of 30 larger than its extent in the y-direction. Hence, it is reasonable to expect considerable similarity between the spot and boundary-layer cases regarding the generation of pressure peaks also.

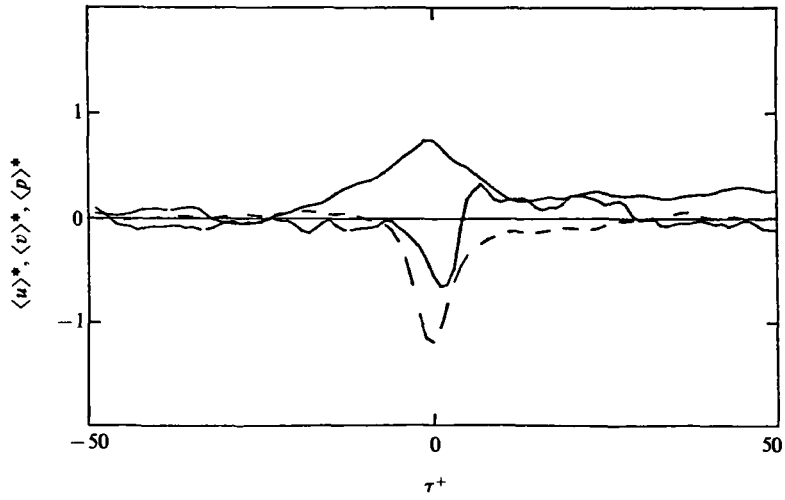

FIGURE 10. Conditional averages of p_w (dashed line), and u (uppermost curve) and v at $y^+ = 15$ for negative pressure-peak events ($k = 2.5$).

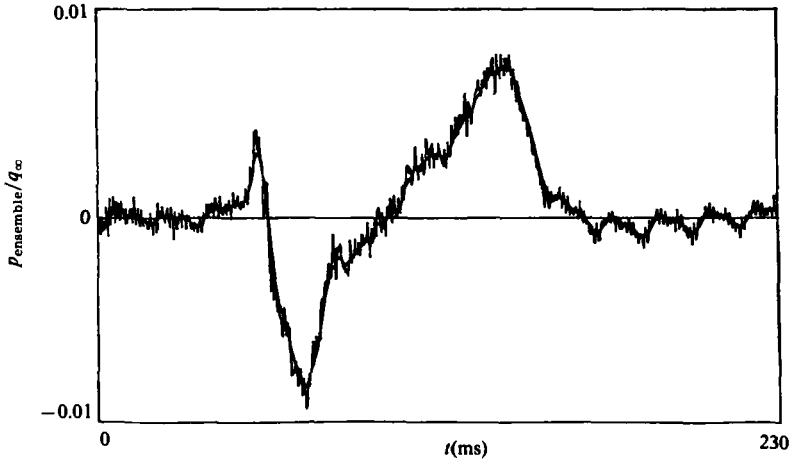

FIGURE 11. Ensemble-averaged pressure signature of 500 spots, and its low-pass filtered counterpart. $x = 1.54$ m, $x_{trig} = 0.29$ m, $U_\infty = 10.1$ m/s. t is delayed 0.090 s from instant of triggering.

Each set of data in the following presentation was constructed from 500 spots. The resulting ensemble-averaged wall-pressure signature (normalized with free-stream dynamic pressure) is shown in figure 11, together with its low-pass filtered counterpart. It is characterized by a small positive peak at the leading edge of the spot, followed by a rapid decrease to a large negative value (-0.009). The central region of the spot can be characterized by a ramp-like increase in pressure to a value of about the same magnitude as the negative peak. This qualitative behaviour is in good agreement with the results of Coles & Savas (1979), although the amplitudes are smaller in the present case. Their negative peak reaches a value of about -0.011 and the positive trailing-edge peak has an amplitude of 0.017 (see their figure 4). The spot pressure signature found by Mautner & Van Atta (1982), however, is considerably different from the present results, despite very similar flow conditions, spot trigger method and position, as well as measurement position. Their signature is dominated

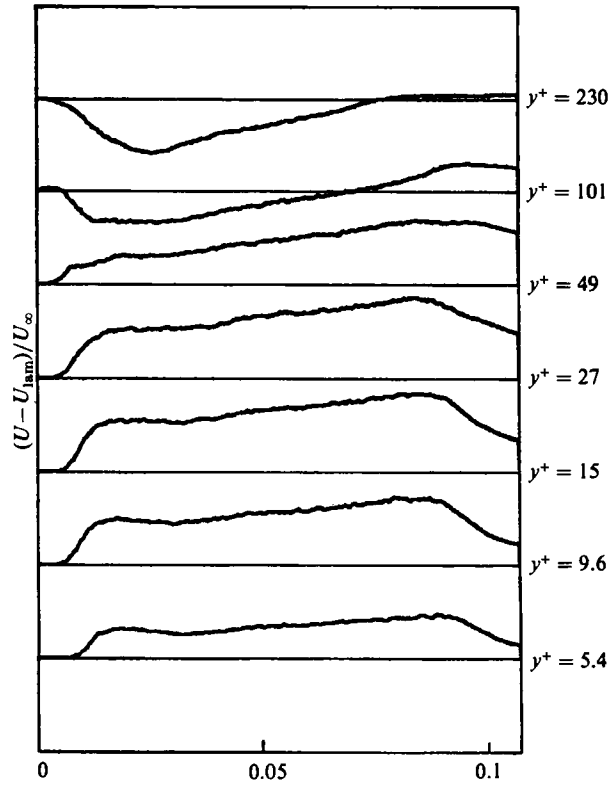

FIGURE 12. Ensemble-averaged velocity signatures of the spot at various distances from the wall (averaged over 500 realizations). $U_\infty = 10.1$ m/s, $x = 1.54$ m. The distance between horizontal lines corresponds to 0.5.

by two large (amplitude of about 0.01) peaks, close to the leading and trailing edges, and a central region of almost constant slightly negative pressure (their figure 3). They used the same type of transducer as in the present case, but with a pinhole mounting. This arrangement was tested here, but was found not to be the cause of the differences in signature appearance. Also initial disturbance duration and amplitude were varied without significant change in the pattern, thus leaving us without any satisfactory explanation. In the present case, the same type of signature appearance was also found at other streamwise positions closer to the generation point. It is also interesting to compare with the results of Cantwell *et al.* (1978), who inferred the wall-pressure pattern from measured velocity data in the plane of symmetry of the spot. They presented the data in terms of a spatial coordinate, that decreases with increasing time, as seen by a fixed observer. In comparison with the present results, the inferred signature lacks the small positive peak near the leading edge, but is characterized by a negative peak near the leading edge, followed by a ramp-like increase to a positive peak near the trailing edge. The present data are, hence, in qualitative agreement with those of Cantwell *et al.*, although the present amplitudes are approximately a factor of two larger.

Velocity signatures from various distances from the wall are shown in figure 12, where the y^+-values were estimated with the friction velocity determined from a Clauser plot of the mean velocity profile. The latter was averaged spatially over the central turbulent region of the spot (roughly 60 % of the interval shown in figure 12)

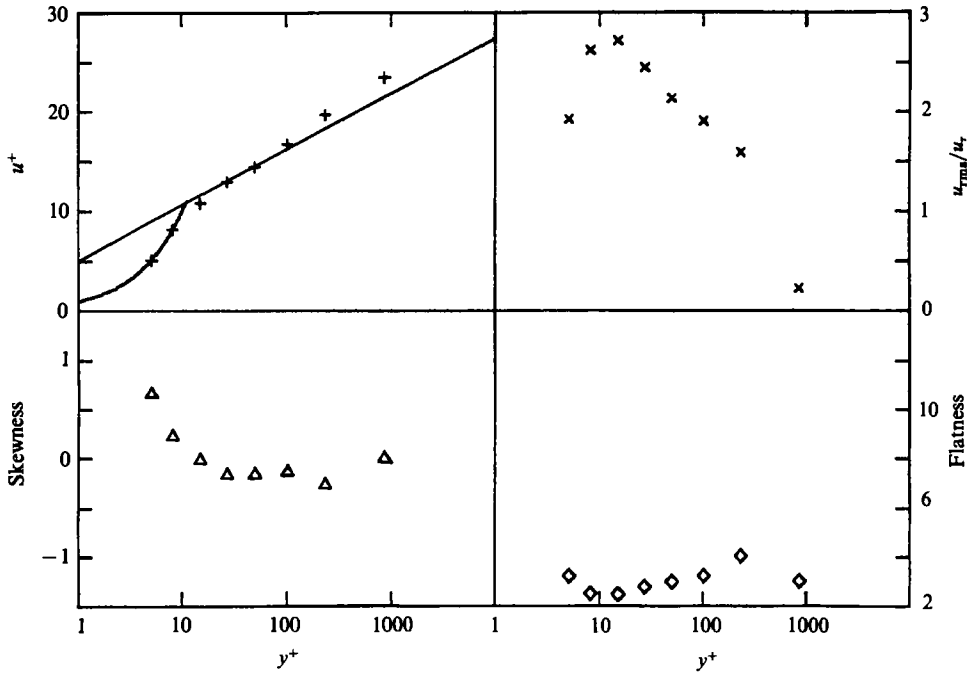

FIGURE 13. Profiles of mean velocity, streamwise turbulence intensity, skewness and flatness in the interior of the spot. $x = 1.54$ m. Straight line in mean velocity plot represents $u^+ = (1/0.41)\ln y^+ + 5.0$.

and ensemble-averaged over 500 spots. The Clauser plot gave a U_∞/u_τ ratio of 23.5 (see figure 13), which is a quite reasonable value for a low-Reynolds-number boundary layer such as this. To study the structure of velocity and pressure fluctuations in the interior of the spot, the ensemble average was subtracted from each realization before further data analysis. The statistical moments of the streamwise fluctuations around the ensemble mean value were then computed in the same manner as the mean velocity. It is quite clear from figure 13 that the similarity between the interior of the spot and the turbulent boundary layer also extends to the streamwise turbulence intensity, skewness and flatness. With the U_∞/u_τ ratio mentioned above the maximum normalized turbulence intensity was found to be 2.73, occurring at about $y^+ = 15$. The skewness and flatness here attained values of -0.02 and 2.5, respectively (cf. figure 1). As an example of the variation in terms of statistical quantities among different spot realizations it may be mentioned that the standard deviation of u_{rms}, as determined from single spots, was less than 8% of the long-time r.m.s. value.

The intensity of the wall-pressure fluctuations (around the ensemble mean) was found to be about 0.0094, when normalized with free-stream dynamic pressure. This is somewhat higher than the value (0.0078) in the boundary-layer case. However, the two become practically identical when normalized with wall shear, which may be the more relevant quantity. The spot case also corresponds to a lower Reynolds number than the boundary-layer case described in §3. The present Reynolds-number difference should, according to Bull & Langeheineken (1981), account for an intensity difference of about 0.001.

The VITA and pressure-peak detection schemes, described in §3, were also applied to the velocity and pressure data from spots. Only the data from $x = 1.54$ m will be described in the following, but data from positions upstream of this were also analysed

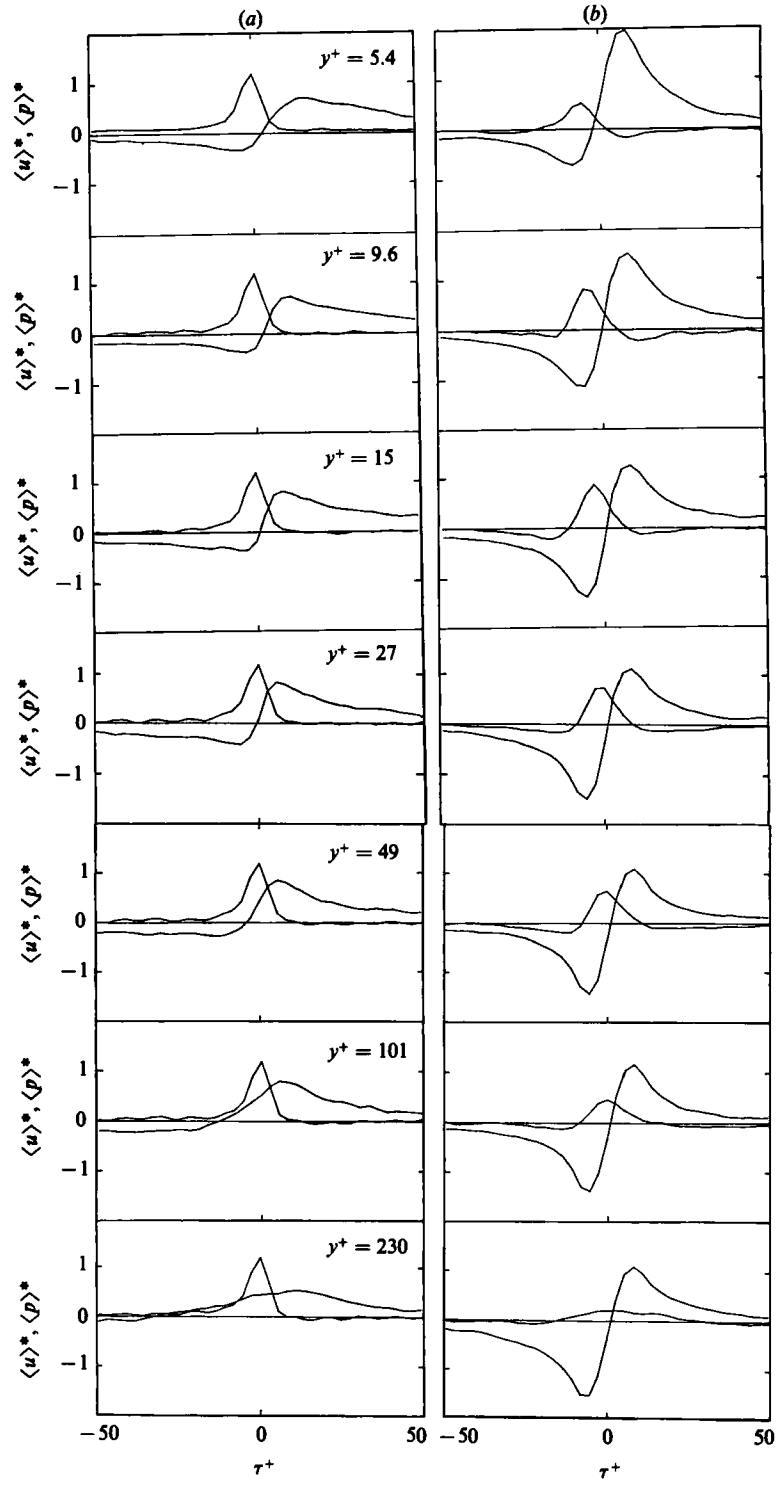

FIGURE 14. Conditional averages of p_w and u at various y^+ positions in the spot for (a) detection of positive pressure peaks ($k = 2.5$), and (b) VITA detection of accelerating events ($K = 1.0$, $T^+ = 22$). $\langle u\rangle^* = \langle u\rangle/u_{\rm rms}$, and $\langle p\rangle^* = \langle p\rangle/kp_{\rm rms}$ in (a) and $\langle p\rangle/p_{\rm rms}$ in (b). τ^+ denotes time, in wall units, relative to the detection time. $x = 1.54$ m.

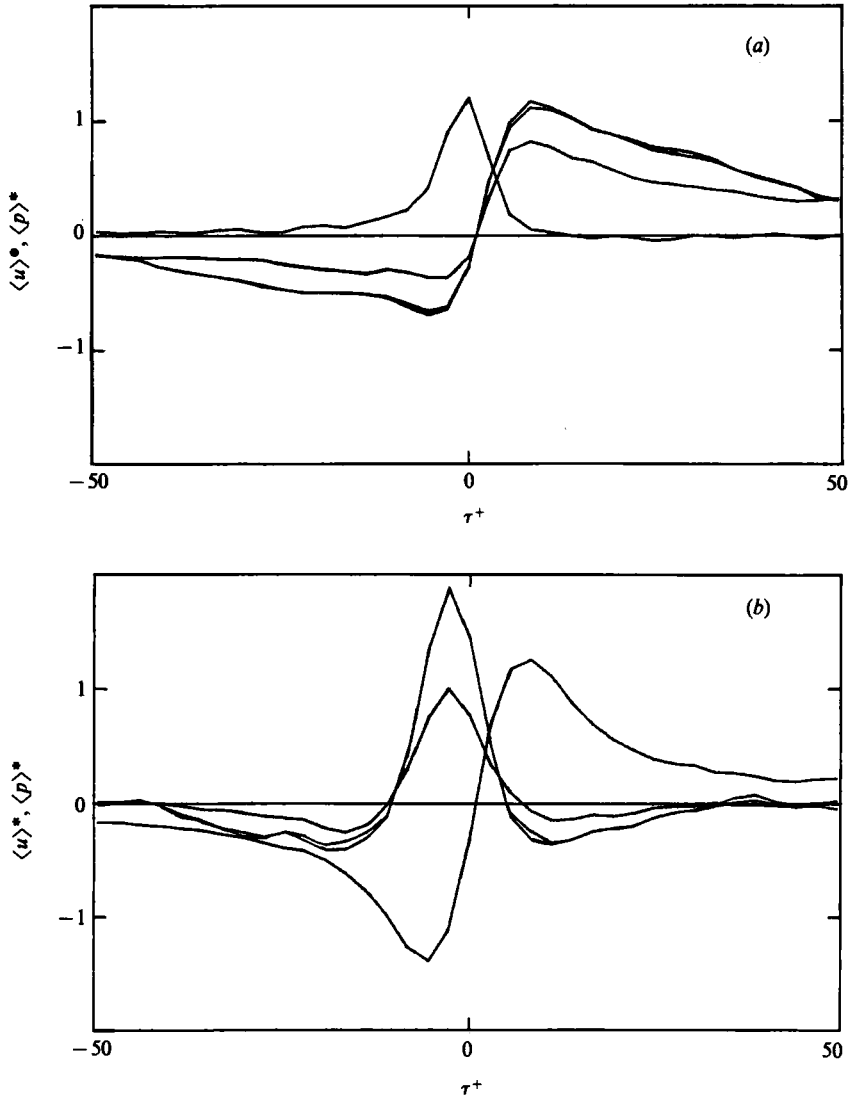

FIGURE 15. Conditional averages of p_w and u at $y^+ = 15$, for zeroth, first and second iteration in the alignment procedure. (*a*) Alignment of u for positive pressure-peak events ($k = 2.5$). (*b*) Alignment of p for accelerating VITA events ($K = 1.0$, $T = 22$).

and were qualitatively similar to those described in the following. The theshold level in the VITA technique was chosen as 1.0, and the averaging time was that which gave the maximum number of detections ($T^+ = 22$). To obtain approximately the same number of positive pressure-peak detections, a threshold $k = 2.5$ was chosen. These are essentially the same parameter values as used in the boundary-layer case.

Results for detection of positive pressure-peak events in the interior of the spots are, in figure 14, compared with velocity and pressure patterns obtained from VITA detection (on u) at various y-positions. Also here (cf. figure 5) one finds the maximum amplitude of the VITA-associated pressure pattern in the buffer region. There is a clear qualitative similarity between the conditional averages at $y^+ = 15$, obtained with the two detection schemes. Also, the general appearance of the results at

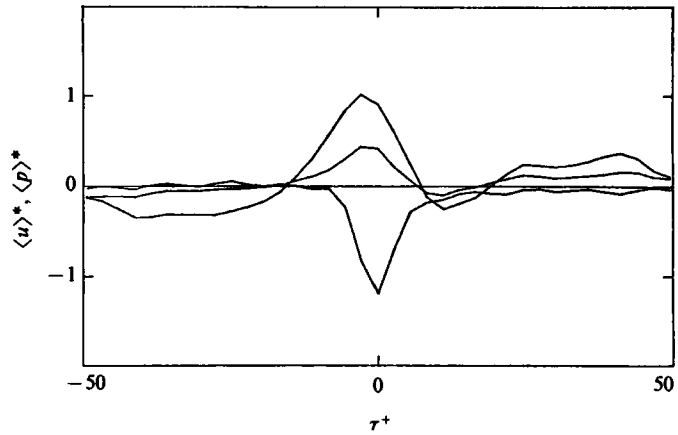

FIGURE 16. Conditional averages of p_w and u for negative pressure-peak events ($k = 2.5$). The velocity patterns represent zeroth and first iteration in the alignment procedure.

different positions exhibit a close resemblance with the boundary-layer results. The alignment technique described in §3.2 was also applied in the spot case and the results from $y^+ = 15$ are shown in figures 15(*a*) and (*b*). The close similarity with the boundary layer case is striking, although not altogether surprising, when one considers that the total (streamwise) extent of the spot is of the order of 100 times larger than the streamwise extent of the detected pressure patterns. The increase in amplitude of the u- and p-patterns after alignment is also about the same as in the boundary-layer case and the correspondence between positive pressure-peaks and VITA events detected in the buffer region is seen to be quite clear also for the spot case.

The relation between negative pressure peaks and flow structures was also investigated (figure 16). The results were found to be very similar to the boundary-layer case, and hence indicative of a coupling to sweep-type motions (cf. figure 10).

5. Discussion and conclusions

The wall-pressure fluctuations at one location are the result of velocity fluctuations in the entire flow domain. The two are coupled through a Poisson's equation, where the source term can be divided into two distinctly different parts. One part is due to the interaction between the mean shear and the velocity fluctuations and is essentially the product of the mean velocity gradient and the streamwise derivative of v. It is linearly related to the velocity fluctuations and can be expected to be large close to the wall where the mean gradient is large. The other part of the source term results from 'turbulence–turbulence' interaction and hence depends non-linearly on the velocity fluctuations. The question of whether the latter type contributes significantly to the intensity of the wall-pressure fluctuations has been a subject of considerable controversy (see e.g. Willmarth 1975) since the early theoretical work of Kraichnan (1956), who concluded that the former represents the dominating sources. A related problem is to establish the location of the flow structures predominantly responsible for the generation of wall-pressure fluctuations. Corcos (1964) analysed this 'pair' of problems and concluded that the linear source terms are only of substantial importance in the inner region of the flow with a centre around $0.2\delta_*$ ($y^+ = 440$ in his case) from the wall.

The fact that large-scale outer-region flow structures give a non-negligible contribution to the long-time r.m.s. value of the wall pressure is evidenced by the high values of propagation velocities found when determined from measurements with two transducers widely apart. Willmarth & Woolridge (1962) determined the propagation velocity from space–time correlations of the wall pressure and found values ranging from $0.56U_\infty$ to $0.83U_\infty$, with increasing values for increasing streamwise separation. Similar results were obtained by Bull (1967), the lowest value in his case being $0.53U_\infty$.

From recent studies (see e.g. Schewe 1983) it has become clear that the large-amplitude pressure patterns propagate with a velocity that falls in the lower part of the above range. Assuming that the pressure patterns are caused by flow structures advected downstream with the local mean velocity, the implication is that these structures are located mainly in the buffer region. This indirect reasoning had earlier been substantiated by simultaneous velocity and pressure measurements in pipe flow by Langeheineken (1981) and to some extent, (as discussed in §3) for boundary-layer flow, by Thomas & Bull (1983).

In the present work, simultaneous pressure and velocity measurements at various distances from the wall were carried out in a moderately high-Reynolds-number boundary-layer flow and in the interior of artificially generated turbulent spots in a laminar boundary layer. By comparing conditional averages obtained from direct detection of high-amplitude positive pressure peaks with those obtained from VITA-detected flow structures, a clear correspondence between shear layers in the buffer region and large positive pressure peaks, in both types of flow, was shown. Here, as well as in the pipe-flow study of Langeheineken (1981), this correspondence was more of a qualitative nature, rather than quantitative, in terms of amplitudes of velocity and pressure patterns. However, by use of an enhanced conditional averaging procedure in which the associated phase-jitter was removed by a cross-correlation technique, the above correspondence was substantially improved. For instance, the amplitude of the pressure signature associated with VITA events detected at $y^+ = 15$ increased by almost a factor of two by the 'alignment' procedure.

The coupling between buffer-region shear layers and high-amplitude positive pressure peaks is a conclusion of considerable generality since it appears to be valid for a low-Reynolds-number pipe flow, for a high-Reynolds-number turbulent boundary layer, as well as for the flow in turbulent spots. Since such shear layers, in general, and VITA events in particular, have been shown to be closely coupled to the turbulence generation mechanisms, this also suggests a link between large wall-pressure peaks and turbulence production.

The present results also give further evidence that the linear terms, representing the interaction between turbulence and mean shear, in the near-wall region are the main contributors to the high-amplitude wall-pressure peaks. Crucial here is the finding (figure 7) that the amplitude of the VITA-associated pressure peak linearly with the amplitude of the velocity pattern. This indicates that the high-amplitude wall-pressure peaks are generated by a linear mechanism through interaction with the mean shear. The importance of the turbulence–mean shear interaction for the generation of large pressure peaks was also substantiated by applying the VITA technique on v, thereby detecting events associated with large negative values of $\partial v/\partial x$. These were found to be quite sensitive to phase-jitter in the conditional averaging process, but yielded a pressure-pattern amplitude, after alignment, that is comparable with that for the 'regular' VITA events.

The large negative peaks were found to be primarily associated with sweep-type

motions, where the maximum negative pressure amplitude occurs during a phase of decreasing u and increasing v, i.e. corresponding to a negative value of $\partial v/\partial x$. This, again, is indicative of the importance of turbulence–mean shear interaction in the near-wall region.

The essential mechanisms for generation of large wall-pressure peaks appear to be identical in transitional turbulent spots and in an equilibrium turbulent boundary layer. This similarity between the two cases was found also to prevail for the intensity, skewness and flatness of the streamwise velocity fluctuations (around the ensemble mean in the spot case). The ensemble averaged wall-pressure signature along the centreline of the spot can be characterized by a small positive peak near the leading edge followed by a rapid decrease to a large negative value and a gradual increase to a similarly large positive peak near the trailing edge. The amplitude of these peaks was found to be about 1 % of the free-stream dynamic pressure, which is roughly the same as the intensity of the wall-pressure fluctuations around the ensemble mean.

We would like to thank Mårten Landahl for many helpful discussions. Support by the ONR under contract N00014-83-K-0227 and partial support by the AFOSR under contract F49620-83C-0019 is gratefully acknowledged.

REFERENCES

ALFREDSSON, P. H. & JOHANSSON, A. V. 1984 *J. Fluid Mech.* **139**, 325.

BLACKWELDER, R. F. 1977 *Phys. Fluids* **20**, S232.

BLACKWELDER, R. F. & KAPLAN, R. E. 1976 *J. Fluid Mech.* **76**, 89.

BULL, M. K. 1967 *J. Fluid Mech.* **28**, 719.

BULL, M. K. & LANGEHEINEKEN, T. 1981 *Mitt. Max-Planck Institut fur Strömungsforschung*, no. 73. Göttingen.

CANTWELL, B., COLES, D. & DIMOTAKIS, P. 1978 *J. Fluid Mech.* **87**, 641.

COLES, D. & SAVAS, O. 1979 In *Proc. First Symp. on Laminar-Turbulent Transition, Stuttgart, 1979* (ed. R. Eppler & H. Fasel), p. 277. Springer.

CORCOS, G. M. 1963 *J. Acoust. Soc. Am.* **35**, 192.

CORCOS, G. M. 1964 *J. Fluid Mech.* **18**, 353.

DINKELACKER, A. & LANGEHEINEKEN, T. 1983 In *Proc. IUTAM Symp. on Structure of Complex Turbulent Shear Flows, Marseille 1982* (ed. R. Dumas & L. Fulachier). Springer.

HUSSAIN, A. K. M. F. 1983 *Phys. Fluids* **26**, 2816.

JOHANSSON, A. V. & ALFREDSSON, P. H. 1982 *J. Fluid Mech.* **122**, 295.

JOHANSSON, A. V. & ALFREDSSON, P. H. 1983 *J. Fluid Mech.* **137**, 411.

KIM, J. 1983 *Phys. Fluids* **26**, 2088.

KIM, J. & MOIN, P. 1986 *J. Fluid Mech.* **162**, 339.

KRAICHNAN, R. H. 1956 *J. Acoust. Soc. Am.* **28**, 378.

LANGEHEINEKEN, T. 1981 *Mitt. Max-Planck Institut für Strömungsforschung*, no. 70. Göttingen.

LINDBERG, P. A., FAHLGREN, M. E., ALFREDSSON, P. H. & JOHANSSON, A. V. 1984 In *Proc. Second IUTAM Symp. on Laminar-Turbulent Transition, Novosibirsk*, 1984 (ed. V. Kozlov). Springer.

MANGUS, J. E. 1984 *Mass. Inst. Tech. Dept. Aeronautics and Astronautics, Lab. Rep.* no. 84–2.

MAUTNER, T. S. & VAN ATTA, C. W. 1982 *J. Fluid Mech.* **118**, 59.

PURTELL, L. P., KLEBANOFF, P. S. & BUCKLEY, F. T. 1981 *Phys. Fluids*, **24**, 802.

RILEY, J. J. & GAD-EL-HAK, M. 1985 In *Frontiers in Fluid Mechanics* (ed. S. H. Davis & J. L. Lumley), p. 123. Springer.

SCHEWE, G. 1983 *J. Fluid Mech.* **134**, 311.

THOMAS, A. S. W. & BULL, M. K. 1983 *J. Fluid Mech.* **128**, 283.

WILLMARTH, W. W. 1975 *Ann Rev. Fluid Mech.* **7**, 13.
WILLMARTH, W. W. & ROOS, F. W. 1965 *J. Fluid Mech.* **22**, 81.
WILLMARTH, W. W. & WOOLRIDGE, C. E. 1962 *J. Fluid Mech.* **14**, 187.
WYGNANSKI, I., SOKOLOV, N. & FRIEDMAN, D. 1976 *J. Fluid Mech.* **78**, 785.
ZILBERMANN, M., WYGNANSKI, I. & KAPLAN, R. E. 1977 *Phys. Fluids* **20**, S258.